Springer

Journal of
Mechanical
Science and
Technology

Journal of Mechanical Science and Technology 22 (2008) 1140~1148

www.springerlink.com/content/1738-494x

Numerical estimation of dynamic behavior of viscoelastic elastomer specimen

Basel M. Seoudi[1], Sang-Hyun Kim[2], H. H. Chun[3] and Inwon Lee[3,*]

[1]*Department of Naval Architecture and Ocean Engineering, Pusan National University, Busan 609-735, Korea*
[2]*Department of Naval Architecture and Ocean Engineering, Inha University, Incheon 402-751, Korea*
[3]*Advanced Ship Engineering Research Center (ASERC), Pusan National University, Busan 609-735, Korea*

(Manuscript Received September 10, 2007; Revised March 17, 2008; Accepted March 18, 2008)

Abstract

Dynamic deformation behavior of a cylindrical specimen made of viscoelastic elastomers was investigated numerically by solving the two-dimensional elastic wave equations. In order to enhance the accuracy of the viscoelastic property calculations, a pseudospectral analysis of two-dimensional elastic wave equation was employed. This allowed us to exclude the use of the form factor derived from the conventional one-dimensional model. Using the present method, an assessment of the conventional form factor concept was attempted. The present two-dimensional method was then utilized to predict a forced vibration response of the elastomer samples under periodic excitation. Obtained numerical results were compared with those using the simplest one-dimensional model. Applicable range of the form factor was examined. Empirical formulas to correct static and dynamic form factors for elastic deformation mode, which are suitable for engineering applications, are suggested.

Keywords: Viscoelastic properties; Form factor; Elastic oscillations; Two-dimensional elastic wave equation

1. Introduction

Viscoelastic properties of polymeric materials are required in various scientific and engineering applications such as polymer science [1, 2], attenuation of sound and vibration [3] and skin friction reduction using compliant coating [4]. For relatively slow processes with characteristic frequencies less than 1 Hz, the materials are characterized usually in terms of relaxation time, which describes a transient response to the excitations on the sample. For faster processes it is convenient to express the such viscoelastic properties as the elasticity modulus E, and the loss tangent μ as functions of frequency.

The elasticity modulus of rubber-like materials varies in a wide range from 10^4 to 10^7 Pa. The loss tangent is defined as a phase lag of material deformation to an applied periodic load ($\mu = \mathrm{Im}\,E^* / \mathrm{Re}\,E^*$), where E^* is a complex module of elasticity. The rate between the energy dissipated during one period of deformation to maximum potential energy of the deformed material directly depends on the loss tangent. The loss tangent μ is close to zero for inviscid (purely elastic) materials, but it can reach quite a large value about $\mu = 0.5$~1 under viscous effect. Additional significant parameter is Poisson's ratio σ, which is the ratio of the lateral contraction to the elongation in an infinitesimally small uniaxial extension. Usually rubbers have $\sigma \approx 0.5$, which implies that their shear modulus is small compared with the volume modulus.

There are quite many techniques to measure viscoelastic properties in the frequency range 20-200Hz. This range is characteristic for noise and vibrations of industrial facilities. The techniques for the frequency range from 200Hz to 10kHz were reported by Fitzgerald and Ferry [5], but their method

*Corresponding author. Tel.: +82 51 510 2764, Fax.: +82 51 581 3718
E-mail address: inwon@pusan.ac.kr
DOI 10.1007/s12206-008-0311-2

is based on very special, complicated apparatus, which is not easily applicable in real practice. As an alternative, Ferry [1] proposed a method based on temperature-frequency analogy of Williams–Landel–Ferry, which converts the temperature dependence of E and μ measured at resonance frequency to the frequency dependence at a fixed temperature. However, this method has essential drawbacks, because not all materials obey this rule; furthermore, the conversion factors are *a priori* unknown. Recently, relatively simple methods have been proposed by Smith et al. [6] and Kulik and Semenov [7] for wide frequency band. The measuring frequency range depends mainly on the loading mass and sensitivity of accelerometers that are used to document the response of the mechanical system subjected to the dynamic test. However, this technique requires the use of a form factor, which depends primarily on the geometrical shape of the samples [2, 8]. For example, let us consider linear stationary deformation, in which case the measured effective elasticity modulus is described by Hooke's law

$$E_{eff} = \frac{F/S}{\Delta H/H}, \tag{1}$$

where F and $S = \pi R^2$ are the applied force and the area of the sample. R and H are the radius and the height of the cylindrical sample, respectively. ΔH is the height change under the applied force. As the ratio H/R increases, E_{eff} tends asymptotically to a constant value E. The ratio $\alpha_E = E/E_{eff}$ is called a form factor. Similarly, in the case of unsteady loading, one can introduce a form factor α_μ to correct the measured loss tangent $\alpha_\mu = \mu/\mu_{eff}$. The values of α_E and α_μ depend on the Poisson ratio σ, and sample geometry. All dependencies are unknown *a priori* and have to be estimated for various sample shapes under tests.

In the present study, an assessment of the form factor concept has been performed. Toward this end, a series of numerical tests have been attempted based on the numerical analysis for a two-dimensional elastic wave equation. The numerical techniques for deformed states are well developed and summarized, for example, in Sadd [9] and Timoshenko and Goodier [10]. Certain difficulties appear in boundary conditions, which can be incompatible to each other in corner points both under static and dynamic loads. For large static deformations, Tsai [11] assumed a parabolic barreling of a sample bonded between two rigid plates, which makes it possible to estimate the form factor without complicated calculations. The barrel shape and the form factor were found by Rosin [12] based on variational principles. However, under dynamic forcing, the sample can change its shape in more complicated manner. In this study, a technique for numerical calculation of the elasticity modulus E and the loss tangent μ as well as the correction factors for the form factors derived from one-dimensional analysis for two practically important setups.

2. Two-dimensional dynamic deformations of bonded cylindrical sample

2.1 Governing equations

Fig. 1 illustrates the viscoelastic sample shape under consideration, a circular cylinder with the radius R. The axial length and the mass of the sample are H and m. The sample consists of the viscoelastic material with the modulus of elasticity E, loss tangent μ and Poisson ratio σ. The sample is attached to the oscillating table on one side and loaded with a mass M on the other side. The oscillating table excites a harmonic oscillation with amplitude A_0 and frequency ω. The load mass M attached on the other side of the sample exhibits the same frequency of oscillation with the amplitude ZA_0 and the phase lag θ.

The displacement of the particle in the sample due to the wave can be described as

$$\vec{\xi} = \zeta(r,z,t)\hat{e}_z + \eta(r,z,t)\hat{e}_r, \tag{2}$$

where $\eta(r,z)$ and $\zeta(r,z)$ are radial and axial displacement components, respectively. The governing equation for a two-dimensional elastic wave in isotropic medium takes the form [13]

$$\frac{\partial^2 \vec{\xi}}{\partial t^2} = C_t^2 \Delta \vec{\xi} + (C_\ell^2 - C_t^2)\nabla\left(\nabla \cdot \vec{\xi}\right), \tag{3}$$

where $C_t^2 = \dfrac{E(1+\mathrm{i}\mu)}{2\rho(1+\sigma)}$, $C_\ell^2 = \dfrac{E(1+\mathrm{i}\mu)(1-\sigma)}{\rho(1+\sigma)(1-2\sigma)}$, $\rho = \dfrac{m}{\pi R^2 H}$. C_t and C_ℓ correspond to the propagation velocities of transverse and longtudinal waves, respectively.

If harmonic excitation is assumed, then Eq. (3) can

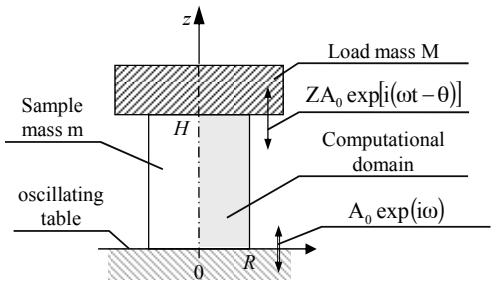

Fig. 1. Schematic diagram of viscoelastic sample.

be written as

$$\begin{aligned} &C_\ell^2\left(r\frac{\partial\eta}{\partial r}-\eta+r^2\frac{\partial^2\eta}{\partial r^2}+r^2\frac{\partial^2\zeta}{\partial r\partial z}\right)\\ &+C_t^2r^2\left(\frac{\partial^2\eta}{\partial z^2}-\frac{\partial^2\zeta}{\partial r\partial z}\right)+r^2\omega^2\eta=0,\\ &C_\ell^2\left(r\frac{\partial^2\eta}{\partial r\partial z}+\frac{\partial\eta}{\partial z}+r\frac{\partial^2\zeta}{\partial z^2}\right)\\ &+C_t^2\left(\frac{\partial\zeta}{\partial r}-\frac{\partial\eta}{\partial z}+r\frac{\partial^2\zeta}{\partial r^2}-r\frac{\partial^2\eta}{\partial r\partial z}\right)+r\omega^2\zeta=0. \end{aligned} \tag{4}$$

The boundary conditions for the cylindrical sample can be written as:

a) Absence of radial displacements at bonded surfaces

$$\eta=0 \quad \text{at} \quad z=0\,, \tag{5}$$

$$\eta=0 \quad \text{at} \quad z=H\,. \tag{6}$$

b) Axial harmonic displacements at the lower and upper surfaces

$$\zeta=A_0e^{i\omega t} \quad \text{at} \quad z=0\,, \tag{7}$$

$$\zeta=ZA_0e^{i(\omega t-\theta)} \quad \text{at} \quad z=H\,. \tag{8}$$

c) Absence of strains at the side surface (at $r=R$)

$$\sigma_{rz}=0\rightarrow\frac{\partial\eta}{\partial z}+\frac{\partial\zeta}{\partial r}=0\,, \tag{9}$$

$$\sigma_{rr}=0\rightarrow(1-\sigma)\frac{\partial\eta}{\partial r}+\sigma\left(\frac{\partial\zeta}{\partial z}+\frac{\eta}{r}\right)=0\,. \tag{10}$$

Additionally, symmetry conditions can be used along the cylinder axis:

$$\eta(r=0)=0,\ \frac{\partial\zeta}{\partial r}(r=0)=0\,. \tag{11}$$

The procedure to obtain E and μ is to solve an inverse problem defined by Eqs. (3), (5)-(10). Toward this end, measured data of the oscillation magnitude ratio Z and the phase delay θ are utilized. A unique solution is obtained with the help of the following compatibility condition:

$$\begin{aligned} &M\frac{\partial^2\zeta}{\partial t^2}=-2\pi\rho C_\ell^2\int_0^R\sigma_{zz}(H,r)\,r\,dr,\\ &MZ\omega^2e^{i(\omega t-\theta)}\\ &=2\pi\frac{E(1+i\mu)(1-\sigma)}{(1+\sigma)(1-2\sigma)}\int_0^R\frac{\partial\zeta}{\partial z}(H,r)\,r\,dr, \end{aligned} \tag{12}$$

which equates internal stress at the upper edge with the pressure developed by the movement of the finite load mass M. The latter part of Eq. (12) is obtained by substituting $\zeta=ZA_0e^{i(\omega t-\theta)}$.

2.2 One-dimensional model equations

Apart from the two-dimensional wave equation in the above, one-dimensional variant needs to be analyzed separately because the major goal of the present study is to estimate the form factor based on the one-dimensional model. In this one-dimensional analysis, the radial deformation component is neglected and the governing equation regarding the axial deformation is solved to get E_{eff} and μ_{eff} as in Kulik and Semenov [7].

The governing equation for the cylindrical sample in Fig. 1 is given as

$$\rho\frac{\partial^2\zeta(z,t)}{\partial t^2}=E_{eff}\left(1+i\mu_{eff}\right)\frac{\partial^2\zeta(z,t)}{\partial z^2}\,, \tag{13}$$

with the boundary conditions of Eqs. (7) and (8) and the following compatibility condition:

$$\frac{M}{S}\frac{\partial^2\zeta}{\partial t^2}=-E_{eff}\left(1+i\mu_{eff}\right)\frac{\partial\zeta}{\partial z} \quad \text{at} \quad z=H\,. \tag{14}$$

Application of harmonic boundary conditions (Eqs. (7) and (8)) leads to frequency domain analysis in terms of harmonic solution. Further reductions of $E_{eff}(f)$ and $\mu_{eff}(f)$ to obtain a correction for the form factor applicable for a variety of E and μ are described in Section 3.

2.3 Solution procedure

To solve the governing equations (Eqs. (3), (5)-(10)) numerically, a pseudospectral approximation of the wave equations with $N_z\times N_r$ mesh points was

used [14]. A grid was set up based on Chebyshev Gauss–Lobatto knots independently in z and r, thereby producing a so-called tensor product grid. Let the rows and columns of the $(N+1)\times(N+1)$ Chebyshev spectral differentiation matrix D_N be indexed from 0 to N. The entries of this matrix are given by the following rules [14, 15] :

$$(D_N)_{00}=\frac{2N^2+1}{6},\ (D_N)_{NN}=-(D_N)_{00},$$
$$(D_N)_{jj}=\frac{-x_j}{2(1-x_j^2)},\ j=1,\ldots N-1, \tag{15}$$
$$(D_N)_{ij}=\frac{c_i}{c_j}\frac{(-1)^{i+j}}{x_i-x_j},\ i\neq j, i, j=1,\ldots N-1,$$

where $x_k=\cos(i\pi/N),\ k=0,1,\cdots,N$ and

$$c_i=\begin{cases}2 & i=0 \text{ or } N\\ 1 & \text{otherwise}\end{cases}. \tag{16}$$

Due to the incompatibility of the boundary conditions in the corner points at $r=R, z=0$, and $r=R, z=H$, where $\partial\zeta/\partial z$ and $\partial\zeta/\partial r$ can be discontinuous, the accuracy of the calculation of the integrals in Eq. (12) is relatively low [16]. However, the corner singularities in these cases are quite weak and a reduction of the error to an admissible value in using relatively small matrix sizes can be done, e.g., by an appropriate coordinate transformation, which condenses the knots at the corners [17]. Toward this end, the following coordinate transformation from x to y was employed:

$$y=\frac{\arctan(ax)}{\arctan(a)}, \tag{17}$$

which mapped the polynomial domain $[-1;1]\times[-1;1]$ onto itself. Here, the scaling factor of a=2 is nondimensional. The knots concentrate at the corners and become more sparse in the bulk of the sample, as the scaling factor a becomes larger. However, when the number of knots is too limited in the bulk of the sample, the form of the deformation cannot be resolved anyway, if N_z and N_r are fixed small. In the numerical tests described in the next section a=2 was used. This value was chosen on a trial basis to produce an "optimal" knot distribution, that is, to minimize values of N_z and N_r for production of the results accurate enough for our purpose in the whole frequency range under study and, hence, to accelerate the calculations. Our tests showed that as the number of knots in each direction is enlarged from 12 to 20, the approximated values of E and μ change less than 1% in the region of interest, which is within an estimated experimental error in measuring the amplitudes and phase shifts of the axial displacement.

Then, a linear coordinate transformation mapped the problem from the polynomial domain $[-1;1]\times[-1;1]$ to the physical domain $[0;H]\times[-R;R]$. Specifically, we consider the mesh $(r_i,z_j), r_i=R\cos\left(\frac{i\pi}{N_r}\right), z_j=\frac{H}{2}\left[\cos\left(\frac{j\pi}{N_z}\right)+1\right],\ i=0,\cdots,N_r, j=0,\cdots,N_z$

Due to the axisymmetry of the problem in R, the use of the whole domain $[-R;R]$ is redundant, so we kept only points r_i with $i=0,\cdots,N_r/2$ (N_r is even) and performed the actual calculations in the domain $[0;H]\times[0;R]$.

Let us represent the functions of displacements $\eta(r_i,z_j)$ and $\zeta(r_i,z_j)$ in the mesh points by the matrices $(\eta)_{i,j}$ and $(\zeta)_{i,j}$ and denote the first discrete derivative operators in r and z as $\bar{D}_r=D_{N_r}/R$ and $\bar{D}_z=2D_{N_z}/H$, respectively. For the sake of simplicity, odd integers for N_r were used in this calculations. Then, due to the axial symmetry of the problem under consideration, we are interested only in the solution at $r\in[0;R]$, in which case the matrix $\bar{D}_r$ can be reduced to the matrices $\bar{\bar{D}}_r$ for the even function $\zeta(r_i,z_j)$ and $\tilde{\bar{D}}_r$ for the odd function $\eta(r_i,z_j)$, of which elements are given as

$$\begin{aligned}&\left(\bar{\bar{D}}_r\right)_{ij}=\left(\bar{D}_r\right)_{ij}+\left(\bar{D}_r\right)_{ik},\\ &i,j=0\ldots(N+1)/2, k=N+1-j,\\ &\left(\tilde{\bar{D}}_r\right)_{ij}=\left(\bar{D}_r\right)_{ij}-\left(\bar{D}_r\right)_{ik},\\ &i,j=0\ldots(N+1)/2, k=N+1-j.\end{aligned} \tag{18}$$

If we reassemble the matrices η and ζ into the column vectors built by the columns of η and ζ written one by one (that is, we represent them in the lexicographic order), the directional derivative matrices may be expressed as tensorial (Kroneker) products and become [15],

$$\begin{aligned}&\bar{D}_r=\bar{\bar{D}}_r\otimes I_z, \tilde{D}_r=\tilde{\bar{D}}_r\otimes I_z,\\ &D_z=I_r\otimes\bar{D}_z,\\ &\bar{D}_{rr}=\bar{\bar{D}}_r^2\otimes I_z, \tilde{D}_{rr}=\tilde{\bar{D}}_r^2\otimes I_z,\\ &D_{zz}=I_r\otimes\bar{D}_z^2,\end{aligned} \tag{19}$$

$\bar{D}_{rz} = \bar{\bar{D}}_r \otimes \bar{D}_z, \tilde{D}_{rz} = \tilde{\bar{D}}_r \otimes \bar{D}_z,$

where I_z and I_r are the unit (N_z+1) and (N_r+1) matrices, respectively. Then, the original system of equations is approximated by the following matrix equation:

$$\begin{bmatrix} C_\ell^2\left(r^2\tilde{D}_{rr}+r\tilde{D}_r - I_r \otimes I_z\right)+C_t^2 r^2 D_{zz}+r^2\omega^2 & \left(C_\ell^2-C_t^2\right)\left(r\tilde{D}_{rz}+D_z\right) \\ \left(C_\ell^2-C_t^2\right)r^2\bar{D}_{rz} & C_t^2\left(r\bar{D}_{rr}+\bar{D}_r\right)+C_\ell^2 r D_{zz}+r\omega^2 \end{bmatrix}\begin{pmatrix}\eta\\ \zeta\end{pmatrix}=0. \quad (20)$$

Boundary conditions were applied explicitly by changing the corresponding rows in the left and right-hand sides of the equations [15] to make inhomogeneous problems, which are then easily solved by the left matrix division. Final approximations of E and μ were obtained by Gauss-Newton iterations of the obtained solutions to satisfy the compatibility condition, Eq. (12). The solution was obtained with a standard MATLAB solver of a system of nonlinear equations with cubic line search algorithm choice.

The solution of Eq. (13) with the boundary conditions Eqs. (7), (8) and (14) can be found in an implicit form analytically [7, 18]. Let us consider for brevity only the first case and assume the solution to be in the following form

$$\zeta = F(z)e^{i\omega t} \quad . \quad (21)$$

Substituting ζ in Eq. (13) gives an ordinary differential equation

$$-\omega^2\rho F(z) = E_{eff}(1+i\mu_{eff})\frac{d^2F}{dz^2}, \quad (22)$$

of which the solution can be written as

$$F(y) = C_1 e^{i\delta z} + C_2 e^{-i\delta z}, \quad (23)$$

where

$$\delta = \omega\sqrt{\frac{\rho}{E_{eff}(1+i\mu_{eff})}} = \omega\sqrt{\frac{\rho}{E_{eff}}}\left[\sqrt{\frac{\sqrt{1+\mu_{eff}^2}-1}{2\left(1+\mu_{eff}^2\right)}}+i\sqrt{\frac{\sqrt{1+\mu_{eff}^2}+1}{2\left(1+\mu_{eff}^2\right)}}\right]. \quad (24)$$

Application of the boundary condition of Eq. (7) leads to

$$C_1 + C_2 = A_0. \quad (25)$$

From the boundary condition Eq. (14), the following equation is obtained:

$$-\frac{M}{S}\omega^2\left(C_1 e^{i\delta H}+C_2 e^{-i\delta H}\right) = C_1\delta e^{i\delta H} - C_2\delta e^{-i\delta H}. \quad (26)$$

Constants C_1 and C_2 can be obtained by solving Eqs. (25) and (26). Substituting C_1 and C_2 into Eqs. (22), (23) and equating $z = H$ gives the displacement of the load mass, which is in the form of $\zeta(H) = ZA_0 e^{i(\omega t-\theta)}$. By arranging the terms, the following equation is obtained:

$$\frac{e^{i\theta}}{Z} = \cos(\delta H) - \frac{M\omega^2}{S\delta E_{eff}\left(1+i\mu_{eff}\right)}\sin(\delta H). \quad (27)$$

In order to make Eqs. (22) and (27) dimensionless, the parameters

$$C = \sqrt{\frac{\rho\omega^2 H^2}{E_{eff}\left(1+i\mu_{eff}\right)}}, \quad m = \rho\pi R^2 H$$

are employed. This yields an implicit equation:

$$\frac{e^{i\theta}}{Z} = \cos(C) - iC\frac{M}{m}\sin(C), \quad (28)$$

which can be further reduced to

$$Z\sqrt{1+\left(C\frac{M}{m}\right)^2}\exp\left[C + i\tan^{-1}\left(C\frac{M}{m}\right) - i\theta\right] = 1. \quad (29)$$

Taking natural logarithm of both sides yields

$$\frac{1}{2}\ln\left[Z^2+\left(\frac{ZCM}{m}\right)^2\right] + C + i\tan^{-1}\left(C\frac{M}{m}\right) - i\theta = 0. \quad (30)$$

Then, a solution of Eq. (30) with respect to complex variable C is easily obtained by a nonlinear equation solver. Equations of one-dimensional model of deformation were solved by using such algorithms of MATLAB as Levenberg-Marquardt and Gauss Newton, both with either mixed quadratic and cubic or only cubic polynomial interpolation and extrapolation line search methods [19].

3. Results and discussion

3.1 Displacement diagrams

Before proceeding to the estimation of form factor, it is worthwhile to examine two-dimensional wave deformation behaviors. Fig. 2 illustrates typical examples of $Z(f)$ and $\theta(f)$ with varying loads mass M from the numerical test for the sample of Fig. 1. The calculations were carried out in a wide frequency range including both the parametric resonance frequency $f_{par} \approx \frac{1}{H}\sqrt{\frac{E}{\rho}\frac{m}{M}}$ [6] and the fundamental resonance frequency $f_{fund} \approx \frac{1}{2H}\sqrt{\frac{E}{\rho}}$. The former depends on the load mass M whilst the latter does not. As the frequency passes each resonance frequency, the phase experiences a gradual shift of 180º. The phase behavior in the vicinity of the parametric resonance depends significantly on M, but at higher frequencies the phase becomes essentially independent of M.

The displacements can be separated by amplitude and phase factors as

$$\eta = \eta_0(r,z)\exp\left[i\omega t + \phi_\eta(r,z)\right], \quad \zeta = \zeta_0(r,z)\exp\left[i\omega t + \phi_\zeta(r,z)\right] \tag{31}$$

Corresponding diagrams of displacement amplitudes and phases for the case with M = 5.41g are shown in Figs. 3 and 4 for frequencies f_{par} and f_{fund}, respectively. In both cases in accordance with the boundary conditions, the radial displacement is absent along the axis of the cylinder ($r = 0$) and at lower and upper edges. At parametric resonance (Fig. 3), the radial displacement shows barrel-like shape reaching maximum value about $\eta_{0,\max} \approx 4A_0$ in the middle of H at the cylinder side surface. The phase of the radial displacement is independent of r and z and equal to 90°. The axial displacement grows monotonically from the lower to upper surface reaching $\zeta_{0,\max} \approx 11A_0$. Amplitudes and phases of ζ are virtually independent of r. Upper part of the sample oscillates with 90° lag with respect to the lower part of the sample.

For the fundamental resonance in Fig. 4, the radial displacement shows two humps, whose amplitudes

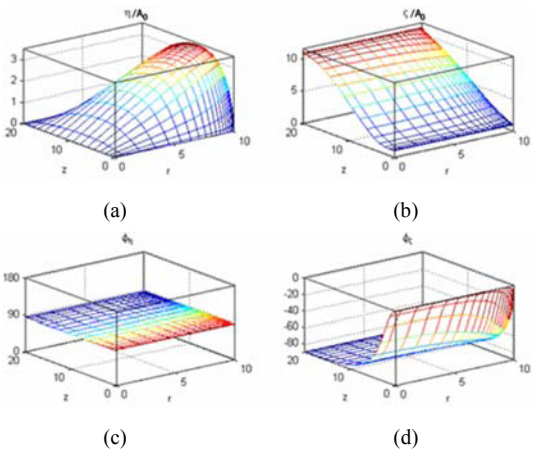

Fig. 3. Distribution of two-dimensional deformation wave at parametric resonance frequency $f = f_{par}$: (a) amplitude of radial deformation, (b) amplitude of axial deformation, (c) phase of radial deformation, (d) phase of axial deformation. Viscoelastic material properties are the same Fig. 2, M/m = 1.

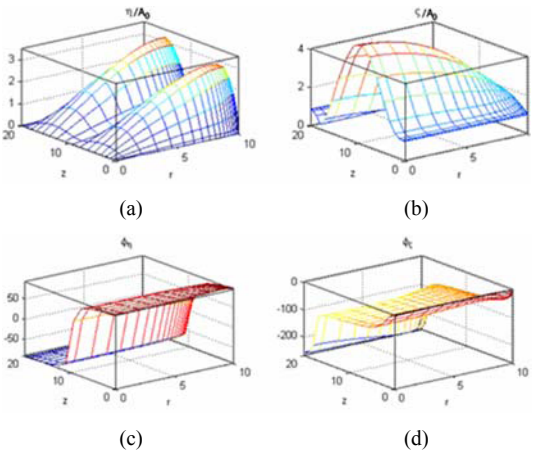

Fig. 4. Distribution of two-dimensional deformation wave at fundamental resonance frequency $f = f_{fund}$: (a) amplitude of radial deformation, (b) amplitude of axial deformation, (c) phase of radial deformation, (d) phase of axial deformation. Viscoelastic material properties are the same Fig. 2, M/m = 1.

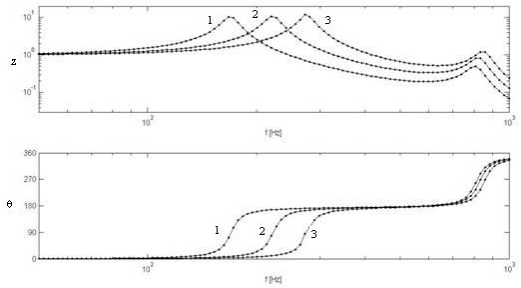

Fig. 2. Response characteristics for a cylindrical sample (R =10mm, H =20mm) with varying load mass: (1) $M = 2m$, (2) $M = m$, and (3) $M = 0.5m$, Viscoelastic material properties ρ =1,000kg/m^3, E =1MPa, μ =0.1 and σ =0.495.

reach maximums at the outer surface. The displacements at the humps oscillate in antiphase indicating the presence of a standing wave. Axial displacement reaches a maximum approximately at $z = H/2$ along the centerline of the sample. Its phase experience abruptly jumps at $z \approx 0$ and $z \approx H$.

A general conclusion which can be drawn from Figs. 3 and 4 is that there should be a limit of quasistationary consideration of the sample barreling in the sense of works [9, 10] somewhere between the frequencies f_{par} and f_{fund}. Above this limit, there hardly exists a way to introduce a more or less universal form factor that is useful for engineering applications. In what follows we outline this frequency limit and will offer a frequency correction for $f < f_{fund}$ or $\theta < 140^\circ$.

3.2 Form factor frequency correction

In the present study, the form factor was calculated by using the procedure in Eq. (32). For E, μ and other parameters are assumed to be independent of frequency as shown in Table 1. The dependencies $Z(f)$ and $\theta(f)$ were calculated by using the two-dimensional model described in Sections 2.1. Then, the estimations $E_{eff}(f)$ and $\mu_{eff}(f)$ corresponding to $Z(f)$, $\theta(f)$ and sample parameters were calculated back by using the one-dimensional inverse problem in Section 2.2.

$$\begin{matrix} E \\ \mu \end{matrix} \xrightarrow{2D\ \mathrm{model}} \begin{matrix} Z(f) \\ \theta(f) \end{matrix} \xrightarrow{1D\ \mathrm{model}} \begin{matrix} E_{eff}(f) \\ \mu_{eff}(f) \end{matrix} \tag{32}$$

Table 1. Parameters of the samples for calculation the form factor in normal mode.

E (MPa)	μ	σ	H (cm)	R/H	ρ (g/cm^3)
0.5,1, 2	0.3	0.495	1	1	1
1	0.1, 0.3, 0.5	0.495	1	1	1
1	0.3	0.30, 0.40, 0.45, 0.495	1	1	1
1	0.3	0.495	0.5,1.0,1.5, 2.0,3.0	1	1
1	0.3	0.495	1	1/4,1/3,1/2,1 ,2,3,4	1
1	0.3	0.495	1	1	1/8,1/4,1/2, 1,2,4,8

Typical curves of the form factors α_E and α_μ for the range $0^\circ < \theta < 140^\circ$ are shown in Fig. 5 for several sets of the governing parameters. As seen, one-dimensional results overestimate E and underestimate μ. Meanwhile, the frequency behavior of the curves looks quite similar. Therefore, one can expect a frequency correction factor which depends on a single similarity variable.

The frequency correction factor $K(f)$ is searched in connection with the following relation:

$$\begin{aligned} \alpha_E(f) &= \frac{E}{E_{eff}(f)} = \frac{E}{E_{eff}(0)} \frac{E_{eff}(0)}{E_{eff}(f)} \\ &= \alpha_E(0) \frac{E_{eff}(0)}{E_{eff}(f)} = \frac{\alpha_E(0)}{K(f)} \end{aligned}, \tag{33}$$

where $\alpha_E(0)$ corresponds to the static form factor. This is because the static form factor is readily obtainable from simple analysis, which is shown in the Appendix. The frequency correction factor $K(f)$ and the form factor for loss tangent for the whole 24 cases listed in Table 1 are plotted in Fig. 6. In the present study, normalization of the frequency has been attempted in terms of a generalized frequency defined by the trial-and-error method as

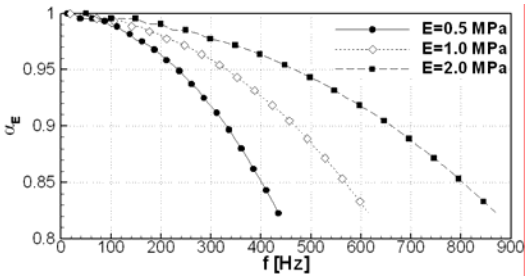

(a)

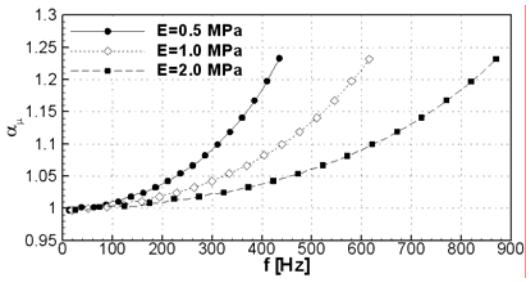

(b)

Fig. 5. Typical calculation result for the form factors for E = 0.5, 1.0, 2.0MPa, μ = 0.3, σ = 0.495, R =10mm, H =20mm; (a) $\alpha_E(f) \equiv E/E_{eff}(f)$, (b) $\alpha_\mu(f) \equiv \mu/\mu_{eff}(f)$.

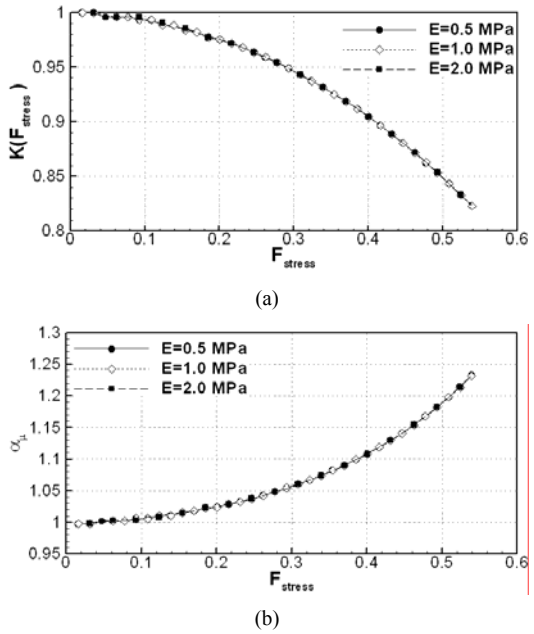

Fig. 6. Correction curves for E and μ versus generalized frequency (normal deformation mode).

$$F_{stress} = \frac{f}{f_{fund}} \frac{\sigma}{1-\sigma} \sqrt{\frac{R}{H}}, \quad f_{fund} = \frac{1}{2H} \sqrt{\frac{E}{\rho}}. \quad (34)$$

As seen, the collapse between different cases encompassing a wide range of parameters E, ρ, σ, H, R/H is remarkably good. The curves of $K(F_{stress})$ and $\alpha_\mu(F_{stress})$ are virtually the same up to $\theta = 90^\circ$ and for the range $90^\circ < \theta < 140^\circ$ the scatter between the curves does not exceed 5%.

It is notable that f_{fund} depends again on E, which is *a priori* unknown in real practice, if we use one-dimensional calculation model. In this case, E_{eff} can be used instead to approximate f_{fund} and appropriate iteration procedures are to be applied to improve the correction factors. We suggest the following empirical formulas of engineering interest, which approximate $K(F_{stress})$ and $\alpha_\mu(F_{stress})$;

$$K(F_{stress}) = 1 - 1.2F_{stress}^2, \quad (35)$$

$$\alpha_\mu(F_{stress}) = 1 + 1.8F_{stress}^2. \quad (36)$$

4. Conclusions

Periodic axial as well as radial deformations of the cylinder loaded by different masses, which are excited at frequency lower than the natural resonance ($\theta < 180^\circ$), were investigated numerically by two-dimensional elastic wave equation. Obtained results were compared with those using the simplest one-dimensional model. It is shown that the dynamic form factor $\alpha_E(f)$ differs from the static analog $\alpha_E(0)$ only slightly. Dynamic form factor $\alpha_\mu(f)$ is also introduced. Empirical formulas of engineering interest for the correction factors $K(f)$ and $\alpha_\mu(f)$ are proposed in connection with generalized frequency. This is toward a correction of the simplest one-dimensional estimate of viscoelastic properties with an acceptable degree of accuracy in a wide parameter combination. The applicability range of the present method is also outlined. The static form factor $\alpha_E(0)$ was calculated by using two-dimensional model of cylinder sample deformation and Hooke's law when the ratio of thickness to diameter changed from 0.1 to 10 and the Poisson ratio was varied from 0.2 to 0.499. For precise measurements in very wide region of experimental parameters, it is necessary to use the two-dimensional model of calculation of viscoelastic properties described in this paper.

Acknowledgments

This research was sponsored by the ERC program (Advanced Ship Engineering Research Center) of MOST/KOSEF.

References

[1] J. D. Ferry, Viscoelastic properties of polymers, John Wiley & Sons, New York, USA, (1961).

[2] E. Riande, R. Diaz-Calleja, M. G. Prolongo, R. M. Masegosa and C. Salom, Polymer viscoelasticity. Stress and strain in practice, Marcel Dekker Inc., New York,USA, (2000).

[3] H-C. Tsai and S-J. Hsueh, Mechanical properties of isolation bearing identified by a viscoelastic method, *Solids and structure,* 38 (2001) 53-74.

[4] V. M. Kulik, S. V. Rodyakin, S-B. Suh, I. Lee and H. H. Chun, Deformation of a viscoelastic coating under the action of convective pressure fluctuations, *Exp. in Fluids*, 38 (5) (2005) 648-655.

[5] E. R. Fitzgerald and J. D. Ferry, Method for determining the dynamic mechanical behavior of gels and solids at audio-frequencies; comparison of mechanical and electrical properties, *J. Colloid Science*, 8 (1) (1953) 1-34.

[6] G. M. Smith, R. L. Beirman and S. J. Zitek, Determination of dynamic properties of elastomers

over broad frequency range, *Experimental Mechanics*, 23 (2) (1983) 158-164.
[7] V. M. Kulik and B. N. Semenov, The two-parametric method for measurements of viscoelastic properties of polymer materials, *Metrologiya*, 4 (1986) 32-38.
[8] C. P. Chen and R. S. Lakes, Apparatus for determining the viscoelastic properties of materials over ten decades of frequency and time, *J. of Rheology*, 33 (8) (1989) 1231-1249.
[9] H. M. Sadd, Elasticity. Theory, Applications, and Numerics, Elsevier Butterworth-Heinemann, Burlington, MA, USA, (2005).
[10] S. P. Timoshenko and J. N. Goodier, Theory of elasticity, McGraw-Hill, London, UK, (1982).
[11] H. H. Tsai, Compression analysis of rectangular elastic layers bonded between rigid plates, *Solids and structures*, 42 (2005) 3395-3410.
[12] G. S. Rosin, Measurement of dynamic properties of acoustic materials, Stroyizdat, Moskow, Russia, (1972).
[13] L. D. Landau and E. M. Lifschitz, Theory of Elasticity, 3rd ed. Pergamon Press, Oxford, UK, (1986).
[14] C. Canuto, M. Y. Hussaini, A. Quarterony and T. A. Zang, Spectral methods in fluid dynamics, Springer Series in Computational Physics, Springer, Berlin, Germany, (1988).
[15] L. N. Trefethen, Approximation theory and numerical linear algebra, in Algorithms for Approximation II (Eds. Mason J, Cox M), Chapman and Hall, London, UK, (1990), 336-361.
[16] V. T. Grinchenko and G. L. Meleshko, Harmonic oscillation and waves in elastic bodies, Naukova Dunka, Kiev,Ukraine, (1981).
[17] T. Tang and M. R. Trummer, Boundary layer resolving pseudospectral methods for singular perturbation problems, *SIAM J. Sci. Comp.*, 17 (2) (1996) 430-438.
[18] V. M. Kulik, B. N. Semenov and S. L. Morosova, Measurement of dynamic properties of viscoelastic materials, *Thermophysics and Aeromechanics*, 14 (2) (2007) 219-230.
[19] R. Fletcher, Practical methods of optimization, Vol. 1, Unconstrained Optimization, John Wiley and Sons, New York, USA, (1980).

Appendix. Calculation of static form factor

The technique described in Sect. 2.2 can be used also to calculate the static modulus of elasticity. In this case Eq. (3) takes the form [13]

$$\Delta\vec{\xi}+\frac{\sigma}{1-2\sigma}\nabla\left(\nabla\cdot\vec{\xi}\right)=0\,, \tag{37}$$

with the boundary conditions Eqs. (5)-(10), if we put $\omega=0$ in Eqs. (7), (8). Instead of dynamic compatibility condition of Eq. (12), the balance of the load mass and internal deformations at the upper edge of the cylinder in the form is used

$$Mg=-\frac{2\pi E\left(1-\sigma\right)}{\left(1+\sigma\right)\left(1-2\sigma\right)}\int_0^R\frac{\partial\zeta}{\partial z}\left(H,r\right)r\,dr\,, \tag{38}$$

where E is real. In a typical experiment, the static deformation A_0 as a function of varying load masses M is measured. The effective modulus of elasticity is defined by Hooke's law :

$$E_{eff}=\frac{Mg}{\pi R^2}\frac{H}{A_0}\,. \tag{39}$$

Then, the static form factor is given by the ratio $\alpha=E/E_{eff}$.

Fig. 7 shows the form factors obtained by the numerical technique of present study and using an analytical formula

$$\alpha=1-K\tanh\frac{1}{K},\quad K=\frac{\sigma}{\sqrt{1+\sigma}}\frac{R}{H}\,. \tag{40}$$

obtained by a variational method for $\sigma\approx0.5$ (Rosin, 1972). This indicates that at $\sigma\approx0.5$ the numerical calculations provide form factor values close to those obtained analytically, while at smaller Poisson ratios the analytical predictions underestimate α especially at $H/D<1$.

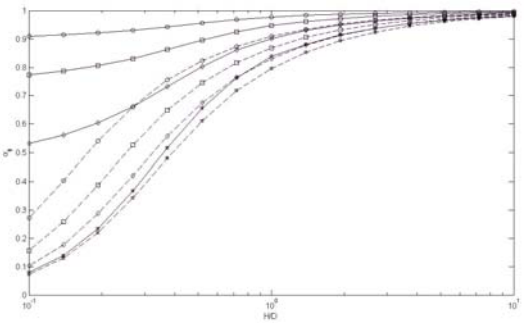

Fig. 7. Static form factor for Poisson ratios: 0.2 (○), 0.3 (□), 0.4 (◊), 0.499 (*) obtained by the numerical calculations (*solid lines*) and by an analytic technique [12] (*dashed lines*).